From the Caribbean to West Africa: Four weeks of continuous dust and marine aerosol profiling with shipborne polarization/Raman lidar — a contribution to SALTRACE

Franziska Rittmeister[1], Albert Ansmann[1], Ronny Engelmann[1], Annett Skupin[1], Holger Baars[1], Thomas Kanitz[2], and Stefan Kinne[3]

[1]Leibniz Institute for Tropospheric Research, Leipzig, Germany
[2]ESTEC, Noordwijk, The Netherlands
[3]Max Planck Institute for Meteorology, Hamburg, Germany

Correspondence to: A. Ansmann (albert@tropos.de)

Abstract. Continuous vertically resolved monitoring of marine aerosol, Saharan dust, and marine/dust aerosol mixtures was performed with multiwavelength polarization/Raman lidar aboard the German research vessel R/V Meteor during a one-month transatlantic cruise from Guadeloupe to Cabo Verde over 4500 km (from 61.5°W to 20°W, mostly along 14.5°N) in April-May 2013, as part of SALTRACE (Saharan Aerosol Long-range Transport and Aerosol-Cloud Interaction Experiment). An overview of measured aerosol optical properties over the tropical Atlantic is given in terms of spectrally resolved particle backscatter and extinction coefficients, lidar ratio, and linear depolarization ratio. Height profiles from the marine boundary layer (MBL) up to the top of the Saharan Air Layer (SAL) are presented. MBL and SAL mean lidar ratios were around 20 and 40 sr. These values indicate clean marine conditions in the MBL and entrainment of marine particles into the lower part of the SAL. In the central and upper parts of the SAL, the lidar ratios were most frequently 50-60 sr and thus typical for Saharan dust. The MBL and SAL mean depolarization ratios were close to 0.05 and between 0.2-0.3, respectively, which reflects almost dust-free conditions in the MBL and the occurrence of a mixture of marine and dust particles in the SAL. The conceptual model, describing the long-range transport and removal processes of Saharan dust over the North Atlantic, is discussed and confronted with the lidar observations along the west-to-east track of the slowly moving research vessel. The role of turbulent downward mixing as an efficient dust removal process is illuminated. In a follow-up article (Rittmeister et al., 2017), the lidar observations of dust extinction coefficient and derived mass concentration profiles are compared with respective dust profiles simulated with three well-established European atmospheric aerosol and dust prediction models (MACC, NMMB/BSC-Dust, SKIRON).

1 Introduction

Mineral dust from desert regions occurs in the atmosphere as surface-near plumes (as part of the boundary-layer aerosol mixture) or elevated free-tropospheric layers. Dust particles can travel over long distances of more than 10000 km in the free troposphere (Haarig et al., 2017a) and can easily be lifted up to heights close to the tropopause during long-range transport

Atmospheric
Chemistry
and Physics
Discussions

(Hofer et al., 2016). As part of the tropospheric background aerosol, dust must be regarded as omnipresent in the northern hemisphere. These particles sensitively influence climatic conditions on the regional to hemispheric scale. Mineral dust from desert regions have a strong impact on the Earth's radiation budget (Myhre and Stordal, 2001; Sokolik et al., 2001; Tegen, 2003; Balkanski et al., 2007) and influences the evolution, lifetime, and radiative properties of liquid-water, mixed-phase, and ice clouds at all tropospheric height levels (Levin et al., 1996; Sullivan et al., 2009; Koehler et al., 2009; Kumar et al., 2009; Seifert et al., 2010; Murray et al., 2012; Hoose and Möhler, 2012; Phillips et al., 2013; Garimella et al., 2014; DeMott et al., 2015).

The Saharan desert is the world's largest mineral dust source (Prospero et al., 2002; Cakmur et. al., 2006; Huneeus et al., 2011) and the transport of mineral dust across the tropical Atlantic is the most prominent example of a powerful long-distance transport of mineral dust (Karyampudi et al., 1999). Dust advection over the tropical Atlantic during the summer months is almost not affected by anthropogenic pollution so that changes in the dust characteristics along the transport ways and dust removal processes can be studied in large detail.

The pioneering work of J. Prospero (Prospero, 1968; Prospero et al., 1972), which he began more than 50 years ago at Barbados in August 1965, triggered numerous dust research activities and well organized field campaigns in western Africa and over the tropical Atlantic. Overviews of these advanced field campaigns conducted during the last 15 years are given in Ansmann et al. (2011) and Ryder et al. (2015). To investigate dust and its climate-relevant aspects, comprehensive dust field experiments (ground-based and airborne activities, in situ measurements combined with active and passive remote sensing) are required with focus on the complex relationship between the microphysical, chemical, shape morphological, optical, radiative and cloud-process-relevant properties of dust particles. The overall aim of these field efforts is to provide improved dust parameterization schemes for weather prediction and climate modeling.

The latest attempt to characterize dust over scales of 10000 km travel distance (equivalent to 6-10 days of travel time) has been performed by the series of well-defined field activities: The Saharan Mineral Dust Experiments SAMUM-1 (southern Morocco, summer 2006) (Heintzenberg, 2009) and SAMUM-2 (Cabo Verde, in the winter and summer of 2008) (Ansmann et al., 2011), and the Saharan Aerosol Long-Range Transport and Aerosol-Cloud-Interaction Experiment SALTRACE (Barbados, in the summers of 2013 and 2014, and the winter of 2014) (Weinzierl et al., 2017). Winter as well as summer-mode dust transport regimes (Schepanski et al., 2009; Ben-Ami et al., 2009) were covered by the two SAMUM-2 and three SALTRACE field phases (Tesche et al., 2011a; Haarig et al., 2017a). Based on the SAMUM-2 observations and simultaneously performed lidar measurements in Amazonia it was clearly demonstrated for the first time that significant amounts of biomass burning smoke are transported towards South America and the Caribbean during the winter half year (Ansmann et al., 2009; Tesche et al., 2011b; Baars et al., 2011).

The dust/smoke layers are advected at comparably low heights, typically below 3 km height, during the winter season. In contrast, almost pure dust plumes leave the African continent in summer. The dust layers reach up to 5-6 km height over western Africa (Tesche et al., 2011a) and the eastern part of the tropical Atlantic. The SAL is then found over Barbados between about 1.5 km and 4 km height (Groß et al., 2015; Haarig et al., 2016, 2017a).

The main goal of the SAMUM and SALTRACE activities was to conduct a detailed vertically resolved characterization of Saharan dust close to the source as well as within the Saharan air layer (SAL) (Karyampudi et al., 1999; Colarco et. al., 2003; Jung et al., 2013) on the way towards the Caribbean, about 5000-8000 km downwind the main source regions. All SAMUM and SALTRACE field sites are shown in Fig. 1. As part of SALTRACE, a unique lidar dataset of aerosol profiles has been acquired

5   aboard the German research vessel R/V Meteor from Guadeloupe to Cabo Verde (Kanitz et al., 2014). The cruise, also shown in Fig. 1, took place from 29 April to 23 May 2013, and thus during the transition period from winter to summer dust transport conditions. The four-week ship cruise offers the opportunity to better link and interpret the SAMUM and SALTRACE results as a whole, but especially the SALTRACE activities. A major contribution to SALTRACE were research flights with the Falcon aircraft of the German Space Center (Chouza et. al., 2015, 2016; Weinzierl et al., 2017). Airborne in situ aerosol observations

10   and remote sensing of aerosol and wind fields were performed in the Cabo Verde regions as well as in the Caribbean during the main SALTRACE field phase in June and July 2013.

A multiwavelength polarization/Raman lidar (Engelmann et al., 2016) aboard R/V Meteor was run continuously to measure height profiles of marine and dust optical and microphysical properties from the marine boundary layer (MBL) up to the top of the Saharan air layer (SAL). The general features of the observations (changing geometrical dust layering properties with

15   distance from Africa) and the optical properties of the SAL dust particles and of the dust-marine aerosol mixture below the SAL are presented in this article. In a follow-up publication, the retrieval of mass concentration profiles separately for dust, marine and smoke aerosol is presented and the retrieved profiles of fine dust and coarse dust extinction coefficients and mass concentrations are compared with simulated profiles obtained by means of well-established European atmospheric transport models (Rittmeister et al., 2017).

20   As a second focus, we compare our R/V Meteor lidar observations with the main features of dust transport and removal over the Atlantic Ocean as described by the conceptual model developed by Karyampudi et al. (1999). We discuss the potential importance of turbulent downward mixing towards the Ocean surface as contribution to dust removal. The tropical North Atlantic between western Africa and the Caribbean can be regarded as an almost ideal natural laboratory to study dust removal by wet (rainout, washout) and dry deposition processes (Colarco et. al., 2003).

25   The article is structured as follows: Section 2 provides information on the ship-based experiment, the lidar, and the observational products. Section 3 presents the main results of the cruise based on case studies and statistical overviews. The data analysis was mainly conducted in the framework of a master thesis project Rittmeister (2015). Section 4 presents the discussion of the conceptual SAL model versus the lidar observations. Concluding remarks are given in Sect. 5.

2   SALTRACE R/V Meteor cruise and instrumentation

30   A shipborne east-west lidar study of the SAL has never been performed before. The first vertically resolved lidar-based study of the SAL across the tropical Atlantic was presented by Karyampudi et al. (1999) based on the space lidar LITE (Lidar In-Space Technology) observation aboard the Space Shuttle Discovery in September 1994 (McCormick et al., 1993). Systematic studies of the east-to-west dust transport with the satellite lidar CALIOP were then presented by Liu et al. (2008a) and Liu et al.

(2008b). Further Saharan dust studies over the tropical Atlantic based on CALIOP measurements can be found in Adams et al. (2012) and Tsamalis et al. (2013). The latter characterized the decay of the Saharan dust amount in terms of layer descent and deposition velocity. Both space lidars (LITE, CALIOP) are so-called standard backscatter lidars. These lidar types allow a precise characterization of dust top and base heights and layering features, but do not permit an in-depth characterization of
5   the dust optical properties as we present here based on the SALTRACE Meteor polarization/Raman lidar observations.

2.1 R/V Meteor cruise

The transatlantic cruise M96 of the German R/V Meteor took place from 29 April to 23 May 2013 starting at Guadeloupe (16° N, 61° W) and ending at Cape Verde (17° N, 25° W). The journey covered a distance of approximately 4500 km (Fig. 1). The containerized OCEANET-Atmosphere platform (Kanitz et al., 2011, 2013) aboard is usually operated during north-south
10   cruises of R/V Polarstern between Bremerhaven, Germany, and Cape Town, South Africa, or Punta Arenas, Chile.

2.2 Polly^{XT}

The multiwavelength Raman/polarization lidar system Polly^{XT} (Engelmann et al., 2016) is the key instrument of the OCEANET-Atmosphere platform and installed inside the container. Polly stands for *POrtabLle Lidar sYstem*. The lidar performed continuous observations during the four-week travel. By means of a two-telescope receiver arrangement for near-range and far-range
15   tropospheric profiling, aerosol profiles are available for the marine boundary layer (MBL) and the lofted SAL. The measurements allow us to study the vertical distribution of dust and marine aerosol particles in large detail. The advanced aerosol lidar enabled us to measure profiles of the particle backscatter coefficients (180° scattering coefficient) at 355, 532, and 1064 nm, particle extinction coefficient at 355 and 532 nm, the respective lidar ratios (extinction-to-backscatter ratios) as well as the particle linear depolarization ratio at 355 and 532 nm (Freudenthaler et al., 2009; Engelmann et al., 2016; Baars et al., 2016).
20   A discussion of the uncertainties in the retrieval products is also given in these articles.

The particle depolarization ratio is the most important parameter in the analysis of the vertical aerosol mixing state (mixing of dust with smoke, haze, and marine aerosols) (Mamouri and Ansmann, 2014, 2017). The approach to separate dust and non-dust aerosol profiles is based on characteristic particle linear depolarization ratios for wet spherical marine aerosols of 0.02–0.03, for urban haze and biomass burning smoke of ≤0.05, and about 0.3 for desert dust at 532 nm. The corresponding
25   analysis of the R/V Meteor lidar observations is given in the follow-up article (Rittmeister et al., 2017).

The almost directly measured and thus basic lidar-derived quantity is however the volume linear depolarization ratio which can be obtained from the calibrated ratio of the cross-to-co-polarized backscatter signal (Freudenthaler et al., 2009). Co and cross denote the planes of polarization (for which the receiver channels are sensitive) parallel and orthogonal to the plane of linear polarization of the transmitted laser pulses, respectively. The volume depolarization ratio is influenced by light depolar-
30   ization by air molecules and aerosol and cloud particles. To obtain the particle depolarization ratio a correction for Rayleigh depolarization effects has to be applied (Freudenthaler et al., 2009).

Atmospheric
Chemistry
and Physics
Discussions

2.3 Sun photometer

The lidar profile observations were accompanied by sun photometer measurements in the framework of the Maritime Aerosol Network (MAN) as part of the Aerosol Robotic Network (AERONET) (Smirnov et al., 2009). The MICROTOPS II measurements provide column-integrated aerosol optical properties at 440, 500, 675, 870, and 936 nm (MAN, 2016). In this work, we
5   will use the 440-870 nm Ångström exponent and 500 nm aerosol optical thickness (AOT). AOT uncertainties are around ± 0.02 for each AOT channel.

2.4 Auxiliary observations and data

Radiosondes for measuring, temperature, humidity, and wind profiles were regularly launched at noon and midnight UTC by the German Weather Service (AWI, 2016). The temperature and pressure profiles are used to compute the Rayleigh backscattering
10   and extinction contributions to the observed lidar return signals. Missing radiosonde information has been filled with GDAS (Global Data Assimilation System) height profiles of temperature and pressure from the National Weather Service's National Centers for Environmental Prediction (NCEP) (GDAS, 2016). Aerosol sources apportionment analysis has been supported by air mass transport tracking with the NOAA (National Oceanic and Atmospheric Administration) HYSPLIT (HYbrid Single-Particle Lagrangian Integrated Trajectory) model (HYSPLIT, 2016) using GDAS meteorological data (Stein et al., 2015). The
15   backward trajectories have been combined with maps of active fires as determined with MODIS (Moderate Resolution Imaging Spectroradiometer) on board the Terra and Aqua satellites (MODIS, 2016).

3   Results

3.1   R/V Meteor cruise overview

Kanitz et al. (2014) provided an overview and first results of the R/V Meteor lidar measurements. Figure 2, taken from that
20   article, shows the 1064 nm range-corrected backscatter signal (a), and the 532 nm volume depolarization ratio (b) for all measurements of the cruise between 2 May and 23 May 2013. The high backscatter values (red and orange in Fig. 2a) in the near range of the lidar indicate the dust-free convective MBL with another dust-free, non-convective marine air layer (MAL) ontop. The MBL top height varied between about 300 and 1000 m height during the cruise. As will be explained below (when discussing Fig. 4), the MAL was part of the convectively active MBL days before the lidar observation. During this active phase
25   convective motions and thus marine particles reached the base of the SAL, and even penetrated into the lower part of the SAL. However, during the lidar observations, the MAL (some kind of a residual layer of the former boundary layer) was no longer convectively active, only the effects (occurrence of marine aerosol up to the SAL base indicated by a low depolarization ratio) were measureable.

Green and yellow colors indicate the lofted SAL up to 5 km height. The numbers 1-4 in Figs. 1 and 2 indicate the ship
30   position where characteristic or key stages of dust layering over the tropical Atlantic were observed. The respective case studies 1-4 are presented and discussed in detail in this and the follow-up article.

Atmospheric
Chemistry
and Physics
Discussions

The SAL can best be identified by the volume linear depolarization ratio shown in Fig.2b. Dust particle are irregularly shaped and cause significant depolarization of backscattered light when linearly polarized laser light is transmitted. As a consequence the shown volume linear depolarization ratio (indicating the overall Rayleigh and particle contributions to depolarization) is mostly between 0.1 and 0.3 in the dust-dominated lofted aerosol layers. In contrast, marine particles in the MBL and MAL

5   have a liquid shell. These spherical particles only cause very low depolarization of backscattered layer light so that the volume depolarization ratio in the marine aerosol layers is close to zero if dust particles are absent.

Figure 3 provides an overview of the aerosol particle optical thickness (AOT) at 500 nm wavelength during the cruise. The daily mean 500 nm AOT ranged from about 0.05 at dust-free pure marine aerosol conditions to 0.7 during a major dust outbreak, observed at Mindeloh, Cabo Verde, at the the end of the cruise (case 1 in Fig. 2). During times with dust (gray-shaded

10   areas in Fig. 3) the AOT was mostly between 0.1–0.3. In addition, the Ångström exponent calculated from sun photometer AOT measurements in the 440–870 nm spectral range is shown in Fig. 3. The Ångström exponent as determined with sun photometer was about 0.7 when the AOT was lowest, confirming the dominance of sea salt particles (7-8 May 2013), and dropped towards very low values when desert dust was present and contributed significantly to the column-integrated aerosol load.

Figure 4 shows the four selected lidar observations of key stages of aerosol layering over the tropical Atlantic. Figure 5

15   provides insight in the origin of the air masses in the marine MBL and the SAL for these four cases.

The dust plume observed on 5 May 2013 (case 4) traveled 7-8 days across the Atlantic before reaching 53°W at relatively low heights. According to the backward trajectories in Figure 5, the dust layer monotonically descended from heights above 4500 m over Africa to 1-2 km height at about 55 °W. The dust layer on 9-10 May (case 3) needed 5-8 days from western Africa to the lidar and contained dust released 8-13 days before reaching the research vessel. The dust layer on 14-15 May (case 2)

20   traveled 7-9 days from the main Saharan dust sources to the research vessel. A strong dust outbreak was finally observed on 23 May at Cabo Verde (case 1). The dust layers arrived at Mindeloh, Cabo Verde, after a travel time of 1 day over the tropical Atlantic and accumulated dust over 3–4 days before.

The most remarkable feature in Fig. 4 is the sharp increase of the volume depolarization ratio at the base height of the SAL. This reflects the strong increase of the dust concentration from negligible dust concentrations in the marine aerosol layers to

25   dust mass concentration of 50–100 μg/m^3 and more within a few meters (Rittmeister et al., 2017). Another interesting aspect is that the MBL top does not coincide with the base height of the SAL over remote Atlantic sites (cases 3 and 4, before 24:00 UTC). The third noticeable finding is the decrease of the SAL depth with distance from Africa. The observed SAL features and associated dust removal aspects are further discussed in Sect. 4.

3.2   Optical properties of dust and marine particles

30   In Fig. 6, the vertical profiles of the derived optical properties of the marine and dust aerosol for the four cases are presented. The basic lidar signals were averaged (over 20–75 minutes) and vertically smoothed with window length of 365 to 458 m to reduce the uncertainty in the products caused by signal noise. Therefore sharp changes in the profile values as visible in Fig. 4 at SAL base obtained with temporal and vertical resolution of 30 s and 7.5 m are considerably smoothed out.

The dust extinction coefficients show values from 50-100 Mm^{-1} in the SAL over the remote Atlantic Ocean. During the major dust outbreak observed on 23 May 2013 over Cabo Verde the dust extinction coefficient reached the 300 Mm^{-1} level. As will be discussed in Rittmeister et al. (2017), extinction coefficient values of 50-100 Mm^{-1} and 300 Mm^{-1} indicate dust mass concentrations of 80-160 $\mu g\ m^{-3}$ and about $500\mu g\ m^{-3}$, respectively. Although Fig. 5 shows that the dusty air masses from Africa crossed fire areas, the analysis showed that mixtures of marine particles and desert dust prevailed throughout the lower troposphere up to SAL top. Contributions by biomass burning smoke were only detected on 14 May 2013 above 2.5 km height (Rittmeister et al., 2017). Obviously these fires at the end of the burning season did not contribute significantly to the observed aerosol mixtures.

Weak spectral dependencies of the SAL backscatter and extinction coefficients in the 355–532 nm wavelength range were observed (see the Ångström exponents in Fig. 6, bsc355/532). This spectral feature is typical for desert dust according to the SAMUM and SALTRACE observations (Tesche et al., 2011a; Groß et al., 2015; Haarig et al., 2017a). The stronger backscatter wavelength dependence for the 532-1064 nm wavelength range (bsc532/1064) is also typical for desert dust plumes after long range transport. Although the backscatter-related Ångström exponent is usually ≥ 1 for the 355–532 nm wavelength range, in rare cases, the Ångström exponent is < 1 as observed in the center of the dust layer on 23 May 2013 (see Fig. 6, case 1, 2–3 km height range). Veselovskii et al. (2016) performed lidar measurements of Saharan dust in Senegal and presented several cases with 532 nm backscatter coefficients significantly higher than the ones at 355 nm. This spectral behavior may be caused by a specific chemical composition of the dust particles (and thus specific refractive index characteristics) and by the proximity to the dust sources and therefore by the presence of a comparably large fraction of large dust particles dominating the measured optical effects. These large coarse-mode particles are no longer present over the Atlantic west of the Cabo Verde islands according to our observations (cases 2–4).

The profiles of the particle lidar ratio (extinction-to-backscatter ratio) and the particle linear depolarization ratio provide information on the mixing of dust and marine aerosol. The lidar ratio increases with height from values close to 20 sr at 532 nm for pure marine aerosols to values of 50-60 sr in the upper part of the SAL (at both wavelengths) indicating pure Saharan dust according to the SAMUM and SALTRACE observations (Tesche et al., 2011a; Groß et al., 2015; Haarig et al., 2017a). With increasing height the marine aerosol fraction decreases. However, the lidar-ratio profiles suggest that vertical exchange processes (and upward transport of marine particles) reach up to the SAL center height.

The SAL depolarization ratios at 355 and 532 nm decrease with distance from Africa from maximum values close to 0.23 at 355 nm and 0.27 at 532 nm (case 1) to values around 0.2 (cases 3 and 4). The difference of about 0.05 between the 532 and 355 nm particle depolarization ratios (as typical for desert dust, case 1) also decreases with distance from Africa, which may be another indication for the steadily increasing fraction of marine particles (causing low depolarization ratios at both wavelengths). For comparison, maximum dust linear depolarization ratios with values close to 0.25 (355 nm) and around 0.3 (532 nm) were also found during SAMUM-1 (Freudenthaler et al., 2009) and during heavy dust outbreaks during SAMUM-2 (Groß et al., 2011).

It should be mentioned, however, that decreasing light depolarization and difference between the 355 and 532 nm depolarization values can also be caused by the continuous removal of large dust particles during long-range transport. Submicrometer

dust particle fraction (fine mode) cause depolarization ratios of around 0.16 (532 nm) and 0.21 (355 nm), whereas the su-permicrometer particle fraction (coarse mode) causes depolarization ratios of 0.35-0.40 (532 nm) and 0.25-0.30 (355 nm) (Mamouri and Ansmann, 2017). Thus, a decrease of the coarse dust fraction is associated with a decrease of the overall dust linear depolarization ratio. On the other hand, if marine particles dry at low relative humidity in the SAL, the depolarization

5 ratio of marine aerosol particles may slightly increase from 0.03 to 0.06–0.08 (Haarig et al., 2017b). This influence complicates the interpretation of the depolarization observation.

The radiosonde profiles of temperature and relative humidity (RH) in Fig. 6 are in good agreement with the lidar observa-tions. The dust layers are drier and warmer (indicated by a strong temperature inversion at SAL base) than the surface-near layers (MBL, trade wind zone). The steady increase of the RH with height in the SAL indicates well-mixed conditions. The

10 moist layer below the SAL always reaches up to the SAL base. These humidity features suggest a significant impact of vertical exchange processes in the marine aerosol layer (MBL + MAL) and the lower part of the SAL on the lowering of the dust concentration during the travel across the tropical Atlantic. The very low depolarization ratio in the MBL+MAL height range then indicates a fast removal of dust from these lowest tropospheric layers.

In the follow-up article, the four cases 1-4 will be further discussed. Mass concentration profiles will be shown in addition

15 and the particle extinction and mass concentration profiles for fine dust, coarse dust, and (total) dust will be compared to respective dust transport simulations (Rittmeister et al., 2017).

Figure 7 provides an overview of layer mean optical properties and contrasts MBL+MAL-related and SAL-related values. The figure includes all analyzed cases (16 cases, sampled on 14 of the 22 cruise days). The MBL+MAL and SAL column values are integrals over the height range from the surface up to the sharp increase of the depolarization ratio (MBL+MAL

20 column values), indicating the SAL base height, and from SAL base up to SAL top, respectively.

Because of the strong backscatter efficiency of marine particles, the marine column backscatter coefficients are much larger than the SAL mean backscatter coefficients (see Fig. 7a). The MBL mean 532 nm extinction values are typically 50–100 Mm^{-1} so that the optical depth is 0.03 to 0.07 for typical MBL layers with depths of 500-700 m (see Fig. 7e). The SAL mean extinction values are found to be, frequently between 40 and 100 Mm^{-1}, but can be much higher during strong dust outbreaks as the

25 23 May case in Fig. 7b indicates.

The MBL mean lidar ratios in Fig. 7c are around 20 sr. These values are typical for pure, undisturbed marine conditions over the remote Atlantic Ocean (far away from islands and continents). These values are in good agreement with a few SAMUM-2 cases of pure marine conditions (Groß et al., 2011) and consistent with SALTRACE observations in the marine layer over Barbados (Groß et al., 2016). The lidar ratios were higher (20-30 sr) in the MBL over Barbados because of efficient downward

30 mixing of dust probably caused by island effects (changed surface roughness, changed surface heating) (Engelmann et al., 2011; Jähn et al., 2016).

The majority of SAL mean dust lidar ratios are 40–50 sr. Here it has to be kept in mind that the SAL column values also include some information from below the SAL because of the 458 m signal smoothing length in the respective backscatter and extinction retrievals. SAL mean lidar ratios around 40 sr clearly indicate the impact of marine particles in the lower part of

35 SAL. For pure dust, the lidar ratio is close to 50-60 sr (Tesche et al., 2011a; Veselovskii et al., 2016).

Atmospheric
Chemistry
and Physics
Discussions

The layer mean depolarization ratio for the MBL+MAL height range indicates dust-free conditions when the value is close
to 0.02–0.03 (Groß et al., 2011) and a slight to moderate contribution by desert dust when the depolarization value is around
0.05-0.07. The exceptional high MBL mean depolarization value of almost 0.2 on 23 May 2013 (see Fig. 7d) is caused by the
proximity of Cabo Verde to the African continent so that a well-defined, clean MBL could not built in the lowest part of the
5   dust layer during the short time period of dust advection over the Atlantic.

The SAL mean depolarization ratios with values around 0.2 were found to be considerably lower than the ones for pure dust
(around 0.31 at 532 nm) as observed during the SAMUM-2 and SALTRACE campaigns (Groß et al., 2011, 2015; Haarig et al.,
2017a). During SAMUM-1 (Freudenthaler et al., 2009) and according to the dust observations in Senegal (Veselovskii et al.,
2016) 532 nm dust depolarization ratios can be as large as 0.35, i.e., when freshly emitted coarse dust particles dominate. Values
10   around 0.2 again indicate a considerable contribution of marine backscatter to the total SAL particle backscatter coefficient.

4   Conceptual dust transport model versus lidar observations

Continuous monitoring of aerosol profiles across the tropical Atlantic with a slowly moving research vessel provides favorable
conditions to investigate the dominant features of the long-range transport dust over the ocean and to check the conceptual
model developed by Karyampudi et al. (1999). According to this model, which is based on the dust transport literature pub-
15   lished in the 1970s to 1990s, hot, dry, dust-laden air masses emerge from the western coast of Africa as a series of large-scale
pulses in the summer months. Associated with easterly wave activity, Saharan dust outbreaks occur as discrete episodic pulses,
which generally last three to five days. Periods of 5-7 days are usually required to cross the Atlantic. The strong temperature
inversion at the base of the SAL limits convective activity and consequently precludes the possibility of strong wet removal
(scavenging of dust particles below and within clouds and removal by wash and rain out), except in disturbance. During phases
20   with favorable conditions for strong cloud developments and convective motions, which easily influence the lowermost 2.5–
3 km of the troposphere (according all our SAMUM and SALTRACE lidar observations), turbulent mixing associated with
strong vertical wind shears, upward venting of sea salt aerosol by the penetrating cumulus clouds can cause downward mixing
and removal of Saharan aerosol dust from the atmosphere. The residual aerosol layer (MAL) located between the SAL base
and the top of the MBL possibly represents a mixture of mineral aerosol from the SAL above and sea salt aerosol from the
25   MBL below.

As the SAL moves away from the continent, it is undercut by the cool, moist and dust-free air of the MBL. This marine
zone includes later on the MAL. These important features of the conceptual model are illustrated in Figs. 8 and 9. Figure 9 is
based on the observed geometrical features of aerosol layering presented in Fig. 4. The sub layers (MBL and MAL) receive
dust particles by vertical downward mixing and mainly be gravitational setting (fallout) from the overlaying SAL, which acts
30   as a large reservoir for insoluble particles. During the westward travel, the SAL base rises and the MBL gradually deepens.
The SAL top over the eastern Atlantic is assumed to lower rapidly due to the rapid depletion of giant particles away from the
west African coastline and is additionally caused by the subsidence associated with the Hadley circulation.

The question now arises: Are these features of the dust transport across the Atlantic as described by the conceptual model in agreement with our shipborne lidar observations? Are there aspects that are not described and/or considered properly but have an impact on dust removal?

The most remarkable feature we observed with the shipborne lidar is the sharp change of the volume linear depolarization
ratio at the base of the SAL within a few meters, from an almost no-dust to an only-dust environment. According to the conceptual model, this sharp drop in the depolarization value (when entering the marine aerosol layers) is attributed to the undercut effect (cool and dust-free air from the north to northeast replaces the dust-laden air which travels from east to west). The trajectories in Fig. 5 show the classical assumption of the conceptual model and support this idea. The trajectories indicate very different air masses in the MBL (arrival height at 500 m) and in the SAL. However, the undercut hypothesis is not
supported by Fig. 10 for the observations over the remote Atlantic sites (cases 3 and 4). Trajectories arriving 250 m below and above SAL base over the lidar are shown. One may argue that trajectories are too uncertain to allow such a detailed interpretation. However, the trajectories show a reasonable scenario and can be brought only in consistency with the lidar observations if we assume a strong and rather efficient removal of Saharan dust when dust was moved from the SAL to the MAL or MBL. For 9 May 2013, both trajectories below and above SAL base height indicate dust (and smoke) air mass transport
from Africa. If sedimentation would be the dominant dust removal process we should observe a smooth and slow increase of the volume depolarization ratio in the MBL/MAL layer up to the SAL base height. In the absence of the undercut effect, only very efficient turbulent downward mixing occurring over hours to days upwind of the lidar site can explain such a strong dust cleansing effect.

Sedimentation processes seem to be in general less important. This is indicated by the almost constant dust extinction
coefficients of 50-100 Mm^{-1} in the SAL layer over the Atlantic west of Cabo Verde (cases 2-4, see Figs. 6 and 7). In contrast, the AOT decreased from values of 0.15–0.2 (around the case-2 site) to 0.05-0.1 (around the case-3 and 4 sites, Fig. 7) as a result of the undercut effect (reduction of the depth of the SAL layer) and downward mixing effects as illustrated in Fig. 9. The weak impact of gravitational settling on dust removal from the SAL is also discussed by Gasteiger et al. (2017)

At the end it is noteworthy to mention that the impact of convective mixing and vertical exchange of dust was also studied
in the framework of SAMUM-2 (Engelmann et al., 2011) (ground-based Doppler lidar studies at Praia, Cabo Verde) and SALTRACE (Jähn et al., 2016) (airborne Doppler lidar observations over the Barbados region in combination with Large Eddy Simulations).

5 Conclusions

In the framework of the SALTRACE project we conducted unique four-week shipborne lidar observations of the SAL during
summer-transport-mode conditions between the Caribbean (4000 km west of Africa) and western Africa (1000-3000 km west of the main Saharan dust sources). The focus was on a detailed characterization of the optical properties of dust particles within the marine layer and the SAL and of the aerosol mixing state in the marine layer and the SAL during early summer dust transport conditions.

Atmospheric
Chemistry
and Physics
Discussions

In addition, lidar profiling over remote oceanic sites provides a favorable opportunity to study dust removal processes. No anthropogenic aerosol source disturbs the comparisons. We checked the conceptual dust transport model and found good agreement with our observations regarding most aspects. However, we concluded also that dust removal by turbulent downward mixing processes may be stronger than emphasized in the conceptual model. Further comparions of our lidar observations with

5   dust modeling will be presented in the follow-up paper (Rittmeister et al., 2017).

6   Data availability

Radiosondes for measuring, temperature, humidity, and wind profiles were regularly launched at noon and midnight UTC by the German Weather Service (AWI, 2016). GDAS (Global Data Assimilation System) height profiles of temperature and pressure of the National Weather Service's National Centers for Environmental Prediction (NCEP) are used, in addition, for our compu-

10   tations of Rayleigh scattering contributions (NOAA's Air Resources Laboratory ARL, https://www.ready.noaa.gov/gdas1.php) (GDAS, 2016). The shown AOT data are available at *http://aeronet.gsfc.nasa.gov/new_web/cruises_new/Meteor_13_1.html* (MAN, 2016). The Maritime Aerosol Network (MAN) is a component of AERONET (Smirnov et al., 2009). The trajectories are calculated with the NOAA (National Oceanic and Atmospheric Administration) HYSPLIT (HYbrid Single-Particle Lagrangian Integrated Trajectory) model (http://ready.arl.noaa.gov/HYSPLIT_traj.php) (HYSPLIT, 2016) using GDAS mete-

15   orological data (Stein et al., 2015). In addition, fires detected by MODIS (Moderate Resolution Imaging Spectroradiometer) on board the Terra and Aqua satellites are used and are avaialble at http://rapidfire.sci.gsfc.nasa.gov/firemaps (MODIS, 2016). The lidar are available at TROPOS. Please contact Ronny Engelmann (ronny@tropos.de) for further questions.

Atmospheric
Chemistry
and Physics
Discussions

References

Adams, A. M., Prospero, J. M., and Zhang, C.: CALIPSO-Derived Three-Dimensional Structure of Aerosol over the Atlantic Basin and Adjacent Continents, J. Climate, 25, 6862-6879, doi:10.1175/jcli-d-11-00672.1, 2012.

Ansmann, A., Baars, H., Tesche, M., Müller, D., Althausen, D., Engelmann, R., Pauliquevis, T., and Artaxo, P.: Dust and smoke trans-
5   port from Africa to South America: Lidar profiling over Cape Verde and the Amazon rainforest, Geophys. Res. Lett., 36, L11802, doi:10.1029/2009GL037923, 2009.

Ansmann, A., Petzold, A., Kandler, K., Tegen, I., Wendisch, M., Müller, D., Weinzierl, B., Müller, T., and Heintzenberg, J.: Saharan mineral dust experiments SAMUM-1 and SAMUM-2: What have we learned?, Tellus B, 63, 403–429, doi:10.1111/j.1600-0889.2011.00555.x, 2011.

10   AWI: Pangaea data base, available at: https://www.pangaea.de/, last access: October, 2016.

Baars, H., Ansmann, A., Althausen, D., Engelmann, R., Artaxo, P., Pauliquevis, T., and Souza, R.: Further evidence for significant smoke transport from Africa to Amazonia, Geophys. Res. Lett., 38, L20802, doi:10.1029/2011GL049200, 2011.

Baars, H., Kanitz, T., Engelmann, R., Althausen, D., Heese, B., Komppula, M., Preißler, J., Tesche, M., Ansmann, A., Wandinger, U., Lim, J.-H., Ahn, J. Y., Stachlewska, I. S., Amiridis, V., Marinou, E., Seifert, P., Hofer, J., Skupin, A., Schneider, F., Bohlmann, S., Foth, A.,
15   Bley, S., Pfüller, A., Giannakaki, E., Lihavainen, H., Viisanen, Y., Hooda, R. K., Pereira, S. N., Bortoli, D., Wagner, F., Mattis, I., Janicka, L., Markowicz, K. M., Achtert, P., Artaxo, P., Pauliquevis, T., Souza, R. A. F., Sharma, V. P., van Zyl, P. G., Beukes, J. P., Sun, J., Rohwer, E. G., Deng, R., Mamouri, R.-E., and Zamorano, F.: An overview of the first decade of PollyNET: an emerging network of automated Raman-polarization lidars for continuous aerosol profiling, Atmos. Chem. Phys., 16, 5111-5137, doi:10.5194/acp-16-5111-2016, 2016.

Balkanski, Y., Schulz, M., Claquin, T., and Guibert, S.: Reevaluation of Mineral aerosol radiative forcings suggests a better agreement with
20   satellite and AERONET data, Atmos. Chem. Phys., 7, 81-95, doi:10.5194/acp-7-81-2007, 2007.

Ben-Ami, Y., Koren, I., and Altaratz, O.: Patterns of North African dust transport over the Atlantic: winter vs. summer, based on CALIPSO first year data, Atmos. Chem. Phys., 9, 7867-7875, doi:10.5194/acp-9-7867-2009, 2009.

Ben-Ami, Y., Koren, I., Rudich, Y., Artaxo, P., Martin, S. T., and Andreae, M. O.: Transport of North African dust from the Bodélé depression to the Amazon Basin: a case study, Atmos. Chem. Phys., 10, 7533-7544, doi:10.5194/acp-10-7533-2010, 2010.

25   Cakmur, R. V., Miller, R. L., Perlwitz, J., Geogdzhayev, I. V., Ginoux, P., Koch, D., Kohfeld, K. E., Tegen, I., and Zender, C. S.: Constraining the magnitude of the global dust cycle by minimizing the difference between amodel and observations, J. Geophys. Res. 111, D06207, doi:10.1029/2005JD005791, 2006.

Chouza, F., Reitebuch, O., Groß, S. Rahm, S., Freudenthaler, V., Toledano, C., and Weinzierl, B.: Retrieval of aerosol backscatter and extinction from airborne coherent Doppler wind lidar measurements, Atmos. Meas. Tech., 8, 2909-2926, doi:10.5194/amt-8-2909-2015,
30   2015

Chouza, F., Reitebuch, O., Benedetti, A., and Weinzierl, B.: Saharan dust long-range transport across the Atlantic studied by an airborne Doppler wind lidar and the MACC model, Atmos. Chem. Phys., 16, 11581-11600, doi:10.5194/acp-16-11581-2016, 2016.

Colarco, P. R., Toon, O. B., Reid, J. S., Livingston, J. M., Russell, P. B., Redemann, J., Schmid, B., Maring, H. B., Savoie, D., Welton, E. J., Campbell, J. R., Holben, B. N., and Levy, R.: Saharan dust transport to the Caribbean during PRIDE: 2. Transport, vertical profiles,
35   and deposition in simulations of in situ and remote sensing observations, J. Geophys. Res., 108, 8590, doi:10.1029/2002JD002659, D19, 2003.

Atmospheric
Chemistry
and Physics
Discussions

DeMott, P. J., Prenni, A. J., McMeeking, G. R., Sullivan, R. C., Petters, M. D., Tobo, Y., Niemand, M., Möhler, O., Snider, J. R., Wang, Z., and Kreidenweis, S. M.: Integrating laboratory and field data to quantify the immersion freezing ice nucleation activity of mineral dust particles, Atmos. Chem. Phys., 15, 393-409, doi:10.5194/acp-15-393-2015, 2015.

Engelmann, R., Ansmann, A., Fruntke, J., Seifert, P., Tesche, M., Althausen, D., Müller, D., Esselborn, M., Lieke, K., and Köhler, C.: Doppler lidar observations of heat–island effects on vertical mixing of dust and smoke over Cape Verde during SAMUM–2, Tellus B, 63, 448–458, doi:10.1111/j.1600-0889.2011.00552.x, 2011.

Engelmann, R., Kanitz, T., Baars, H., Heese, B., Althausen, D., Skupin, A., Wandinger, U., Komppula, M., Stachlewska, I. S., Amiridis, V., Marinou, E., Mattis, I., Linné, H., and Ansmann, A.: The automated multiwavelength Raman polarization and water-vapor lidar PollyXT: the neXT generation, Atmos. Meas. Tech., 9, 1767-1784, doi:10.5194/amt-9-1767-2016, 2016.

Freudenthaler, V., Esselborn, M., Wiegner, M., Heese, B., Tesche, M., Ansmann, A., Müller, D., Althausen, D., Wirth, M., Fix, A., Ehret, G., Knippertz, P., Toledano, C., Gasteiger, J., Garhammer, M., and Seefeldner, M.: Depolarization ratio profiling at several wavelengths in pure Saharan dust during SAMUM 2006, Tellus B, 61, 165–179. doi: 10.1111/j.1600-0889.2008.00396.x, 2009.

Garimella, S., Huang, Y. W., Seewald, J. S., and Cziczo, D. J.: Cloud condensation nucleus activity comparison of dry- and wet-generated mineral dust aerosol: the significance of soluble material, Atmos. Chem. Phys., 14, 6003-6019, doi:10.5194/acp-14-6003-2014, 2014.

Gasteiger, J., Groß, S., Sauer, D., Haarig, M., Ansmann, A., and Weinzierl, B.: Particle settling and vertical mixing in the Saharan Air Layer as seen from an integrated model, lidar, and in situ perspective, Atmos. Chem. Phys., 17, 297-311, doi:10.5194/acp-17-297-2017, 2017.

GDAS: Global Data Assimilation System, meteorological data base, available at: https://www.ready.noaa.gov/gdas1.php, last access: October, 2016.

Groß, S., Tesche, M., Freudenthaler, V., Toledano, C., Wiegner, M., Ansmann, A., Althausen, D., and Seefeldner, M.: Characterization of Saharan dust, marine aerosols and mixtures of biomass-burning aerosols and dust by means of multi-wavelength depolarization and Raman lidar measurements during SAMUM 2, Tellus B, 63, 706-724, doi:10.1111/j.1600-0889.2011.00556.x, 2011.

Groß, S., Freudenthaler, V., Schepanski, K., Toledano, C., Schäfler, A., Ansmann, A., and Weinzierl, B.: Optical properties of long-range transported Saharan dust over Barbados as measured by dual-wavelength depolarization Raman lidar measurements, Atmos. Chem. Phys., 15, 11067-11080, doi:10.5194/acp-15-11067-2015, 2015.

Groß, S., Gasteiger, J., Freudenthaler, V., Müller, T., Sauer, D., Toledano, C., and Ansmann, A.: Saharan dust contribution to the Caribbean summertime boundary layer - A lidar study during SALTRACE, Atmos. Chem. Phys. Discuss., doi:10.5194/acp-2016-246, in review, 2016.

Haarig, M., Althausen, D., Ansmann, A., Klepel, A., Baars, H., Engelmann, R., Groß, S., and Freudenthaler, V.: Measurement of the linear depolarization ratio of aged dust at three wavelengths (355, 532 and 1064 nm) simultaneously over Barbados, EPJ Web of Conferences, 119, 18009, ILRC 27, DOI: 10.1051/epjconf/201611918009, 2016.

Haarig, M., Ansmann, A., Althausen, D., Klepel, A., Groß, S., Freudenthaler, V., Farrell, D. A., Engelmann, R., Baars, R., S. P. Burton, Mamouri, R.-E., Marinou, E., and Gasteiger, J.: Triple-wavelength depolarization-ratio profiling with lidar of Saharan dust over Barbados during SALTRACE 2013 and 2014, Atmos. Chem. Phys., SALTRACE special issue, in preparation, 2017a.

Haarig, M., Ansmann, A., Althausen, and Gasteiger, J.: Linear depolarization ratio of dried marine particles: SALTRACE lidar observations and modeling, Atmos. Chem. Phys., SALTRACE special issue, in preparation, 2017b.

Heintzenberg, J.: The SAMUM–1 experiment over Southern Morocco: Overview and introduction, Tellus B, 61, 2-11, doi:10.1111/j.1600-0889.2008.00403.x, 2009.

Atmospheric
Chemistry
and Physics
Discussions

Hofer, J., Althausen, D., Abdullaev, S. F., Engelmann, R., and Baars, H.: Central Asian Dust Experiment (CADEX): Multiwavelength Polarization Raman Lidar Observations in Tajikistan, EPJ Web of Conferences, 119, 18006, ILRC 27, DOI: 10.1051/epjconf/201611918006, 2016.

Hoose, C. and Möhler, O.: Heterogeneous ice nucleation on atmospheric aerosols: a review of results from laboratory experiments, Atmos. Chem. Phys., 12, 9817-9854, doi:10.5194/acp-12-9817-2012, 2012

Huneeus, N., Schulz, M., Balkanski, Y., Griesfeller, J., Prospero, J., Kinne, S., Bauer, S., Boucher, O., Chin, M., Dentener, F., Diehl, T., Easter, R., Fillmore, D., Ghan, S., Ginoux, P., Grini, A., Horowitz, L., Koch, D., Krol, M. C., Landing, W., Liu, X., Mahowald, N., Miller, R., Morcrette, J.-J., Myhre, G., Penner, J., Perlwitz, J., Stier, P., Takemura, T., and Zender, C. S.: Global dust model intercomparison in AeroCom phase I, Atmos. Chem. Phys., 11, 7781-7816, doi:10.5194/acp-11-7781-2011, 2011.

HYSPLIT: HYbrid Single-Particle Lagrangian Integrated Trajectory model, backward trajectory calculation tool, available at: http://ready.arl.noaa.gov/HYSPLIT_traj.php, last access: October, 2016.

Jung, E., Albrecht, B., Prospero, J. M., Jonsson, H. H., and Kreidenweis, S. M.: Vertical structure of aerosols, temperature, and moisture associated with an intense African dust event observed over the eastern Caribbean, J. Geophys. Res.: Atmospheres, 118, 4623-4643, doi:10.1002/jgrd.50352, 2013.

Jähn, M., Muñoz-Esparza, D., Chouza, F., Reitebuch, O., Knoth, O., Haarig, M., and Ansmann, A.: Investigations of boundary layer structure, cloud characteristics and vertical mixing of aerosols at Barbados with large eddy simulations, Atmos. Chem. Phys., 16, 651-674, doi:10.5194/acp-16-651-2016, 2016.

Kanitz, T., Seifert, P., Ansmann, A., Engelmann, R., Althausen, D., Casiccia, C., and Rohwer, E. G.: Contrasting the impact of aerosols at northern and southern midlatitudes on heterogeneous ice formation, Geophys. Res. Lett., 38, L17802, doi:10.1029/2011GL048532, 2011.

Kanitz, T., Ansmann, A., Seifert, P., Engelmann, R., Kalisch, J., and Althausen, D.: Radiative effect of aerosols above the northern and southern Atlantic Ocean as determined from shipborne lidar observations, J. Geophys. Res. Atmos., 118, 12,556–12,565, doi:10.1002/2013JD019750, 2013.

Kanitz, T., Engelmann, R., Heinold, B., Baars, H., Skupin, A., and Ansmann, A.: Tracking the Saharan Air Layer with shipborne lidar across the tropical Atlantic, Geophys. Res. Lett., 41, 1044–1050, doi:10.1002/2013GL058780, 2014.

Karyampudi, V. M., Palm, S. P., Reagen, J. A., Fang, H., Grant, W. B., Hoff, R. M., Moulin, C., Pierce, H. F., Torres, O., Browell, E. V., Melfi, S. H.: Validation of the Saharan Dust Plume Conceptual Model Using Lidar, Meteosat, and ECMWF Data, Bull. Amer. Meteor. Soc., 80, 1045–1075, doi:10.1175/1520-0477(1999)080<1045:VOTSDP>2.0.CO;2, 1999.

Koehler, K. A., Kreidenweis, S. M., DeMott, P. J., Petters, M-D., Prenni, A. J., and Carrico, C. M.: Hygroscopicity and cloud droplet activation of mineral dust aerosol, Geophys. Res. Lett., 36, L08805, doi:10.1029/2009GL037348, 2009.

Kumar, P., Sokolik, I. N., and Nenes, A.: Parameterization of cloud droplet formation for global and regional models: including adsorption activation from insoluble CCN, Atmos. Chem. Phys., 9, 2517-2532, doi:10.5194/acp-9-2517-2009, 2009.

Levin, Z., Ganor, E., and Gladstein, V.: The effects of desert particles coated with sulfate on rain formation in the eastern Mediterranean, J. Appl. Met., 35, 1511-1523, doi:10.1175/1520-0450(1996)035<1511:teodpc>2.0.co;2, 1996.

Liu, D., Wang, Z., Liu, Z., Winker, D., and Trepte, C.: A height resolved global view of dust aerosols from the first year CALIPSO lidar measurements, J. Geophys. Res., 113, D16214, doi:10.1029/2007JD009776, 2008a.

Liu, Z., Omar, A., Vaughan, M., Hair, J., Kittaka, C., Hu, Y., Powell, K., Trepte, C., Winker, D., Hostetler, C., Ferrare, R., and Pierce, R.: CALIPSO lidar observations of the optical properties of Saharan dust: A case study of long-range transport, J. Geophys. Res., 113, D07207, doi:10.1029/2007JD008878, 2008b.

Atmospheric
Chemistry
and Physics
Discussions

Mamouri, R. E. and Ansmann, A.: Fine and coarse dust separation with polarization lidar, Atmos. Meas. Tech., 7, 3717-3735, doi:10.5194/amt-7-3717-2014, 2014.

Mamouri, R.-E., and Ansmann, A.: Separation of fine-mode dust, coarse-mode dust, and non-dust aerosol components with polarization lidar: Atmos. Meas. Tech., SALTRACE special issue, in preparation.

5   MAN: Maritime Aerosolo Network: MAN aerosol data base, available at: http://aeronet.gsfc.nasa.gov/new_web/cruises_new/Meteor_13_1.html, last access: October, 2016.

McCormick, M. P., Winker, D. M., Browell, E. V., Coakley, J. A., Gardner, C. S., Hoff, R. M., Kent, G. S., Melfi, S. H., Menzies, R. T., Platt, C. M. R., Randall, D. A., and Reagan, J. A.: Scientific Investigations Planned for the Lidar In-Space Technology Experiment (LITE). Bull. Amer. Meteor. Soc., 74, 205–214, doi: http://dx.doi.org/10.1175/1520-0477(1993)074<0205:SIPFTL>2.0.CO;2, 1993.

10 MODIS: MODIS fire information, available at: http://rapidfire.sci.gsfc.nasa.gov/firemaps, last access: October, 2016.

Murray, B. J., O'Sullivan, D., Atkinson, J. D., and Webb, M. E.: Ice nucleation by particles immersed in supercooled cloud droplets, Chem. Soc. Rev., 41, 6519-6554, doi:10.1039/c2cs35200a, 2012.

Myhre, G. and Stordal, F.: Global sensitivity experiments of the radiative forcing due to mineral aerosols, J. Geophys. Res. 106, 18193-18204, doi:10.1029/2000JD900536, 2001.

15 Prospero, J. M.: Atmospheric dust studies on Barbados, Bull. Amer. Meteorol. Soc., 49, 645-652, 1968.

Prospero, J. M., and Carlson, T. N.: Vertical and areal distribution of Saharan dust over the western equatorial North Atlantic Ocean, J. Geophys. Res., 77, 5255-5265, 1972

Prospero, J. M., Ginoux, P., Torres, O., Nicholson, S. E. and Gill, T. E.: Environmental characterization of global sources of atmospheric soil dust identified with the Nimbus 7 Total Ozone Mapping Spectrometer (TOMS) absorbing aerosol product, Rev. Geophys. 40,
20 doi:10.1029/2000RG000095, 2002.

Rittmeister, F.: The African dust and smoke layer over the tropical Atlantic during the spring season of 2013: Ship-based lidar observations from Guadeloupe to Cape Verde, University Master Thesis, 69 pages, Universität Leipzig, Germany, 2015.

Rittmeister, F., Ansmann, A., Engelmann, R., Basart, S., Benedetti, A., Spyrou, C., Skupin, A., Baars, H., Seifert, P., and Kanitz, T.: From the Caribbean to West Africa: Ship-based lidar profiling of dust and marine aerosol versus aerosol transport modeling, Atmos. Chem. Phys.,
25 SALTRACE special issue, in preparation, 2017.

Ryder, C. L., McQuaid, J. B., Flamant, C., Rosenberg, P. D., Washington, R., Brindley, H. E., Highwood, E. J., Marsham, J. H., Parker, D. J., Todd, M. C., Banks, J. R., Brooke, J. K., Engelstaedter, S., Estelles, V., Formenti, P., Garcia-Carreras, L., Kocha, C., Marenco, F., Sodemann, H., Allen, C. J. T., Bourdon, A., Bart, M., Cavazos-Guerra, C., Chevaillier, S., Crosier, J., Darbyshire, E., Dean, A. R., Dorsey, J. R., Kent, J., O'Sullivan, D., Schepanski, K., Szpek, K., Trembath, J., and Woolley, A.: Advances in understanding mineral dust and
30 boundary layer processes over the Sahara from Fennec aircraft observations, Atmos. Chem. Phys., 15, 8479-8520, doi:10.5194/acp-15-8479-2015, 2015.

Phillips, V. T. J., DeMott, P. J., Andronache, C., Pratt, K. A., Prather, K. A., Subramanian, R., and Twohy, C.: Improvements to an empirical parameterization of heterogeneous ice nucleation and its comparison with observations, J. Atmos. Sci., 70, 378-409, doi:10.1175/JAS-D-12-080.1, 2013

35 Schepanski, K., Tegen, I., and Macke, A.: Saharan dust transport and deposition towards the tropical northern Atlantic, Atmos. Chem. Phys., 9, 1173-1189, doi:10.5194/acp-9-1173-2009, 2009.

Atmospheric
Chemistry
and Physics
Discussions

Seifert, P., Ansmann, A., Mattis, I., Wandinger, U., Tesche, M., Engelmann, R., Müller, D., Pérez, C., and Haustein, K.: Saharan dust and heterogeneous ice formation: eleven years of cloud observations at a central European EARLINET site, J. Geophys. Res., 115, D20201, doi:10.1029/2009JD013222, 2010.

A. Smirnov, Holben, B. N., Slutsker, I., Giles, D. M. McClain, C. R., Eck, T. F., Sakerin, S. M., Macke, A., Croot, P., Zibordi, G., Quinn, P. K., Sciare, J., Kinne, S., Harvey, M., Smyth, T. J., Piketh, S., Zielinski, T., Proshutinsky, A., Goes, J. I., Nelson, N. B., Larouche, P., Radionov, V. F., Goloub, P., Krishna Moorthy, K., Matarrese, R., Robertson, E. J., and Jourdin, F.: Maritime Aerosol Network as a component of Aerosol Robotic Network, J. Geophys. Res., 114, D06204, doi:10.1029/2008JD011257, 2009.

Sokolik, I. N., Winker, D. M., Bergametti, G., Gillette, D. A., Carmichael, G., Kaufman, Y. J., Gomes, L., Schütz, L., and Penner, J. E.: Introduction to special section: Outstanding problems in quantifying the radiative impacts of mineral dust, J. Geophys. Res., 106, 18015-18028, doi:10.1029/2000JD900498, 2001.

Stein, A. F., Draxler, R. R., Rolph, G. D., Stunder, B. J. B., Cohen, M. D., and Ngan, F.: NOAA's HYSPLIT Atmospheric Transport and Dispersion Modeling System. Bull. Amer. Meteorol. Soc., 96, 2059–2077, doi: 10.1175/BAMS-D-14-00110.1, 2015

Sullivan, R. C., Moore, M. J. K., Petters, M. D., Kreidenweis, S. M., Roberts, G. C., and Prather, K. A.: Effect of chemical mixing state on the hygroscopicity and cloud nucleation properties of calcium mineral dust particles, Atmos. Chem. Phys., 9, 3303-3316, doi:10.5194/acp-9-3303-2009, 2009.

Tegen, I.: Modeling the mineral dust aerosol cycle in the climate system, Quat. Sci. Rev., 22, 1821-1834, doi:10.1016/S0277-3791(03)00163-X, 2003.

Tesche, M., Groß, S., Ansmann, A., Müller, D., Althausen, D., Freudenthaler, V., and Esselborn, M.: Profiling of Saharan dust and biomass-burning smoke with multiwavelength polarization Raman lidar at Cape Verde, Tellus B, 63, 649–676, doi:10.1111/j.1600-0889.2011.00548.x, 2011a.

Tesche, M., Müller, D., Groß, S., Ansmann, A., Althausen, D., Freudenthaler, V., Weinzierl, B., Veira, A., and Petzold, A.: Optical and microphysical properties of smoke over Cape Verde inferred from multiwavelength lidar measurements. Tellus B, 63, 677–694. doi:10.1111/j.1600-0889.2011.00549.x, 2011b.

Tsamalis, C., Chédin, A., Pelon, J., and Capelle, V.: The seasonal vertical distribution of the Saharan Air Layer and its modulation by the wind, Atmos. Chem. Phys., 13, 11235-11257, doi:10.5194/acp-13-11235-2013, 2013.

Veselovskii, I., Goloub, P., Podvin, T., Bovchaliuk, V., Derimian, Y., Augustin, P., Fourmentin, M., Tanré, D., Korenskiy, M., Whiteman, D. N., Diallo, A., Ndiaye, T., Kolgotin, A., and Dubovik, O.: Retrieval of optical and physical properties of African dust from multiwavelength Raman lidar measurements during the SHADOW campaign in Senegal, Atmos. Chem. Phys., 16, 7013-7028, doi:10.5194/acp-16-7013-2016, 2016.

Weinzierl, B., Ansmann, A, Prospero, J. M., Althausen, D., Benker, N., Chouza, F., Dollner, M., Farrell, D., Fomba, W. K., Freudenthaler, V., Gasteiger, J., Groß, S., Haarig, M., Heinold, B., Kandler, K., Kristensen, T. B., Mayol-Bracero, O.-L., Müller, T., Reitebuch, O., Sauer, D., Schäfler, A., Schepanski, K., Spanu, A., Tegen, I., Toledano, C., Walser, A.: The Saharan Aerosol Long-range TRansport and Aerosol Cloud Interaction Experiment (SALTRACE): overview and selected highlights, Bull. Amer. Meteorol. Soc., doi:10.1175/BAMS-D-15-00142.1, in press, 2017.
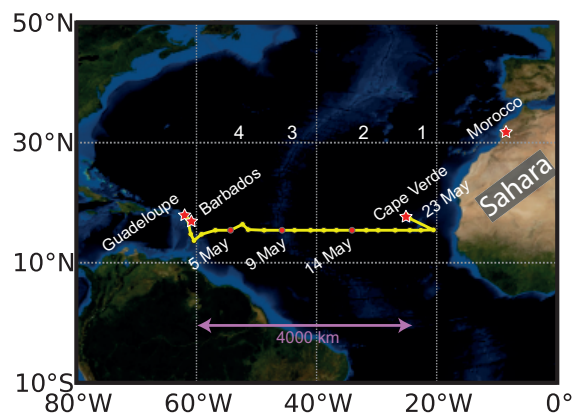
Figure 1. Cruise track of the R/V Meteor from Guadeloupe (29 April 2013) to Cape Verde (23 May 2013) plotted as a thick yellow line (Kanitz et al., 2014). The SAMUM-1 (Morocco), SAMUM-2 (Cape Verde), and SALTRACE (Barbados) field sites are marked by red stars. Red circles and dates (5, 9, 14 and 23 May) indicate the locations of four distinct lidar observations (numbered as 1,2,3, and 4 throughout this paper and the follow-up article). The observations of these key stages of dust layering are discussed in detail in Sect. 3.
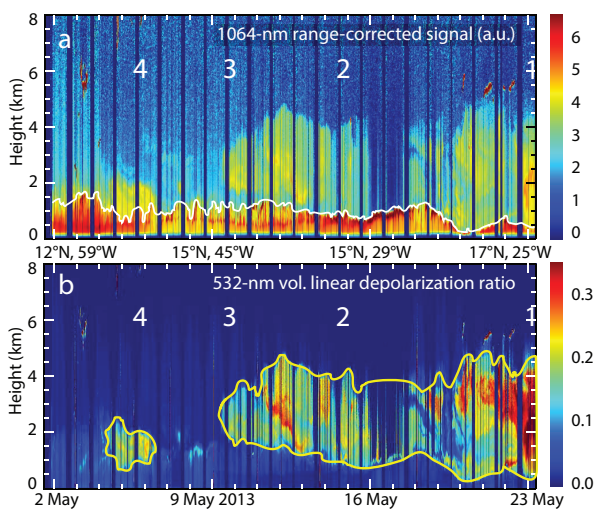
Figure 2. (a) Dust-free marine aerosol layer (MBL + MAL, mostly red, top of MBL + MAL is indicated by a white line) and lofted SAL (bluish, green, and yellow) over the tropical Atlantic between Guadeloupe and Cabo Verde and (b) base and top heights of the SAL indicated by a yellow contour line. The composites are based on lidar measurements of the (a) range-corrected backscatter signal at 1064 nm, and (b) the volume linear depolarization ratio at 532 nm. The figure is taken from Kanitz et al. (2014). Measurement breaks around 1200 LT (blue vertical lines) are due to high sun elevation so that the lidar had to be shut down. Numbers 1-4 indicate the locations of key lidar observations discussed below.
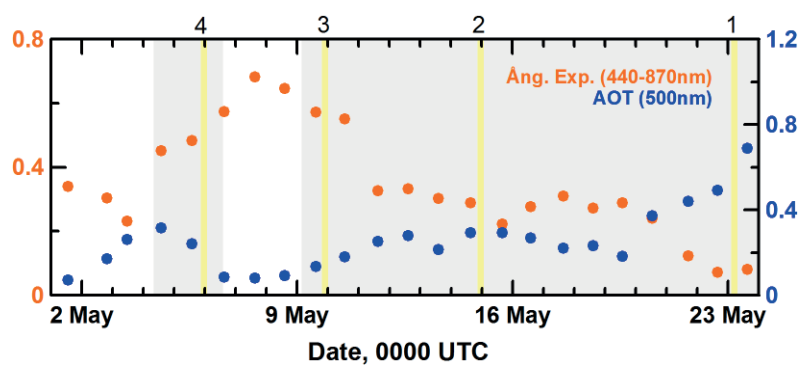
Figure 3. Time series of daily averaged AERONET/MAN sun photometer observations aboard R/V Meteor of aerosol optical thickness (AOT) (blue circles) and Ångström exponent (orange circles) for the 29 April–24 May 2013 period, level-2.0 AOT). The gray-shaded areas indicate the two time periods with lofted dust. The yellow vertical lines indicate the key observational cases 1–4 (given also as numbers on top of the plot).
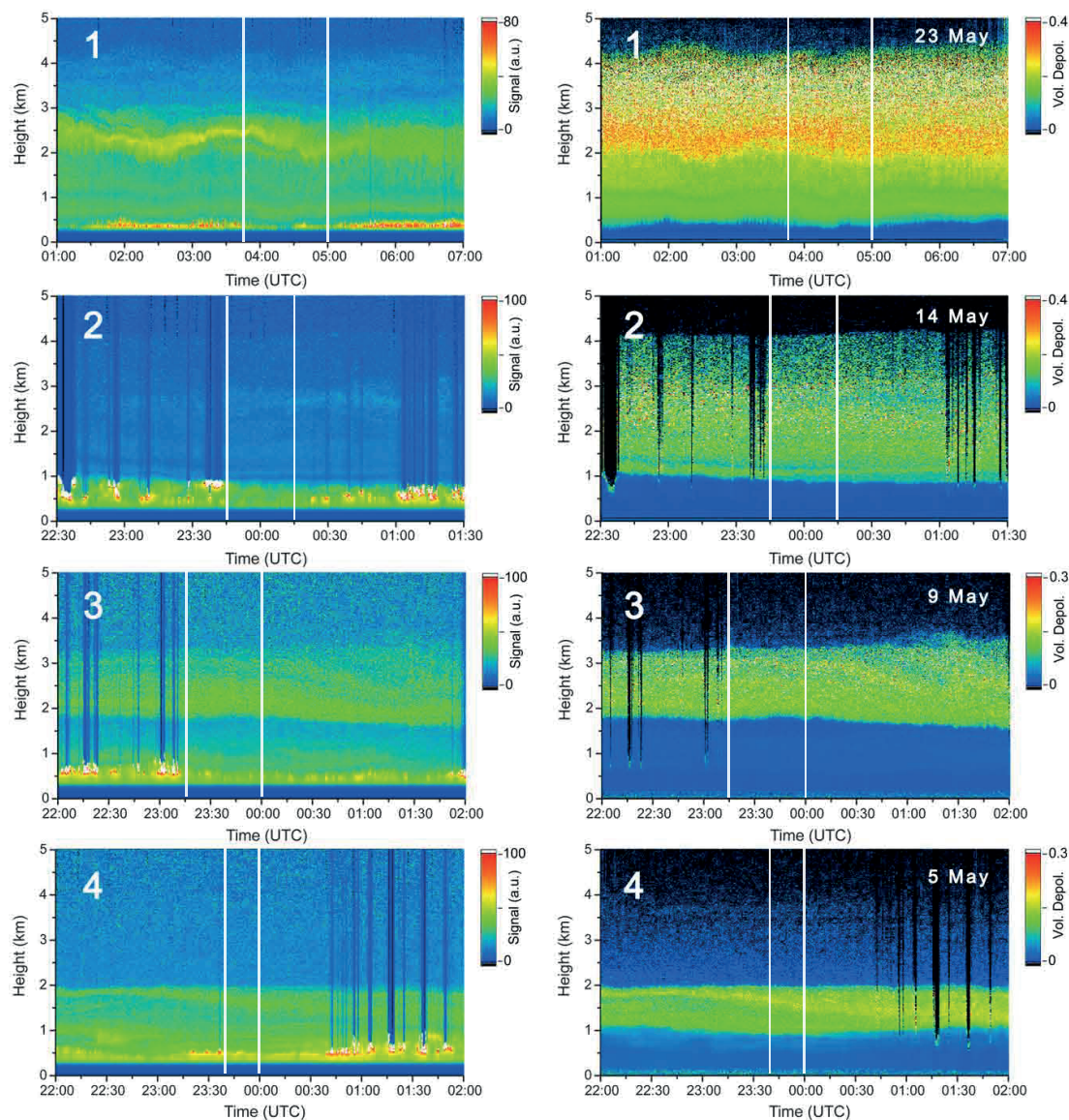
Figure 4. SAL (base height at 400 m, case 1; 1 km, case 2; 1.8 km, case 3; 1 km, case 4) above the convective MBL (white to red spots at the MBL top show trade wind cumulus clouds) and another dust–free layer (marine air layer, MAL). Four distinct lidar measurement sessions on 23 May 2013 (case 1), 14–15 May 2013 (case 2), 9–10 May 2013 (case 3), and 5–6 May 2013 (case 4) are shown in terms of 532 nm range-corrected signal (left) and 532 nm volume linear depolarization ratio (right). Temporal and vertical resolution is 30 s and 7.5 m, respectively. The blue area from the surface to about 250 m height in the left panels indicate the zone with incomplete overlap between the laser beam and the receiver field of view. Blue areas in the right panel indicate dust–free to almost dust-free layers. Vertical lines indicate the signal averaging periods for which the profiles of optical properties in Fig. 6 are calculated.
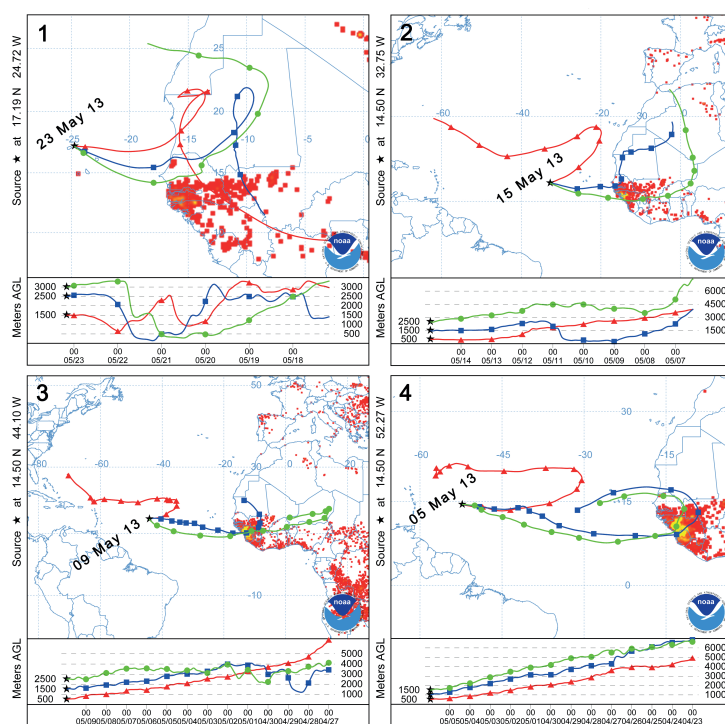
Atmospheric
Chemistry
and Physics
Discussions

Figure 5. Five-day to 13-day HYSPLIT backward trajectories for 23 May 2013, 04:00 UTC (case 1), 15 May 2013, 00:00 UTC (case 2), 9 May 2013, 23:00 UTC (case 3), and 5 May 2013, 23:00 UTC (case 4). Arrival height level of 500 m is within the marine boundary layer. The arrival heights of 1500-3000 m are in the SAL. In addition, fires (red dotes) detected by MODIS on board the Terra and Aqua satellites are shown accumulated over a 10-day period each (21–30 April 2013 for cases 3 and 4, 11–20 May 2013 for case 2, and 21–30 May 2013 for case 1).
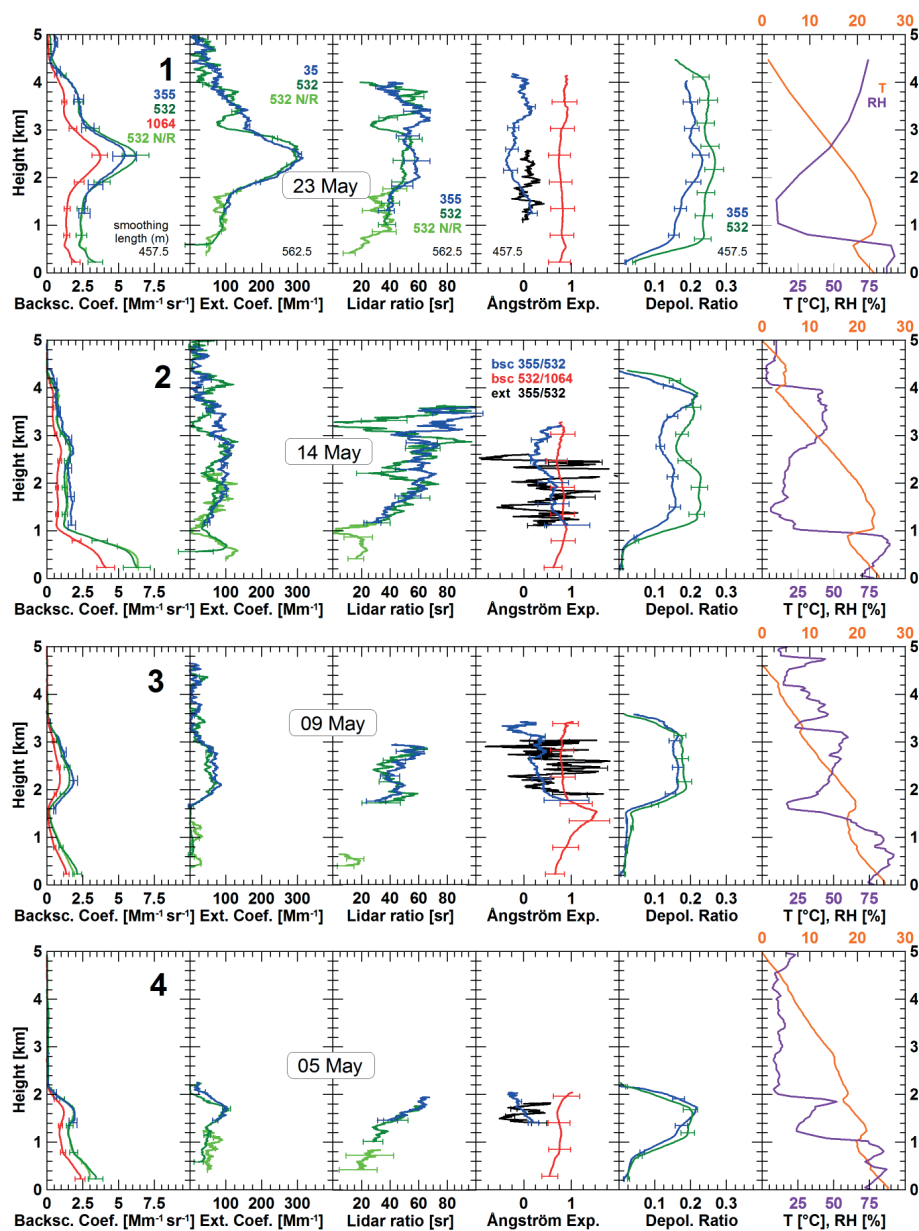
Figure 6. Profiles of the particle backscatter coefficient, extinction coefficient, extinction-to-backscatter ratio (lidar ratio), backscatter-related (bsc) and extinction-related (ext) Ångström exponent, particle linear depolarization ratio, and temperature and relative humidity (from radiosonde, except 23 May, GDAS) for the time periods on 23 May 2013, 03:45–05:00 UTC (case 1), 14–15 May 2013, 23:45–00:15 UTC (case 2), 9 May 2013, 23:15–24:00 UTC (case 3), and 5 May 2013, 23:40–24:00 UTC (case 4). The label 532 N/R denotes the 532 nm near-range receiver channel. The vertical signal smoothing window length for the profiles of backscatter coefficient and particle linear depolarization ratio is 365.0 m, the rest is smoothed with 457.5 m window length. The signal averaging periods are indicated by white horizontal lines in Fig. 4.
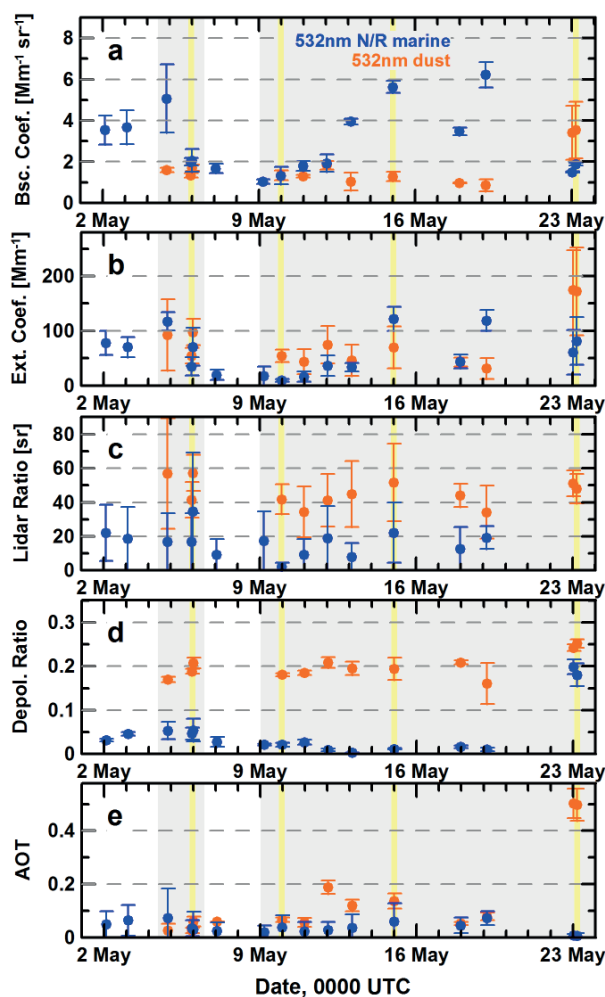
Figure 7. Layer mean values of (a) particle backscatter coefficient, (b) extinction coefficient, (c) lidar ratio, (d) linear depolarization ratio, and (e) aerosol optical thickness (AOT) for the marine aerosol layer (MBL + MAL, blue circles) and the lofted SAL (orange circles). Standard deviations show the combined effect of retrieval uncertainty and variability within the respective layers.

Atmospheric
Chemistry
and Physics
Discussions

Figure 8. Sketch of the westward dust transport in the lofted SAL which is undercut by clean trade winds (dust-free MBL + MAL) according to the dust plume conceptual model of Karyampudi et al. (1999). See text for more details.
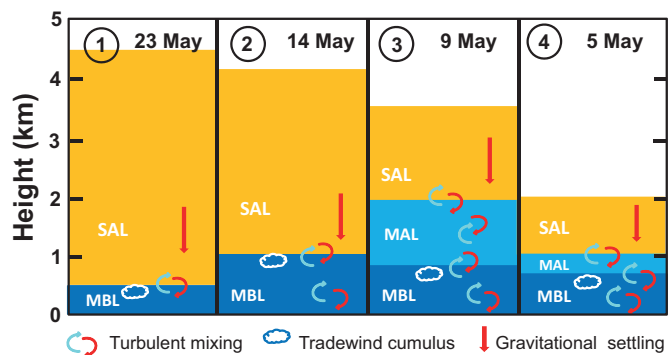

Figure 9. Sketch of dust layering (dust layers in orange) according to the lidar observations in Fig. 4. The R/V Meteor lidar measurements were performed about 1000 km (case 1), 1700 km (case 2), 3300 km (case 3), and 4300 km (case 4) west of the African coast. SAL, MBL, and MAL denote Saharan air layer, marine boundary layer (topped with cumulus clouds), and dust-free marine air layer. Gravitational settling widely controls the removal of dust from the SAL, turbulent downward mixing the removal from the MAL and MBL.
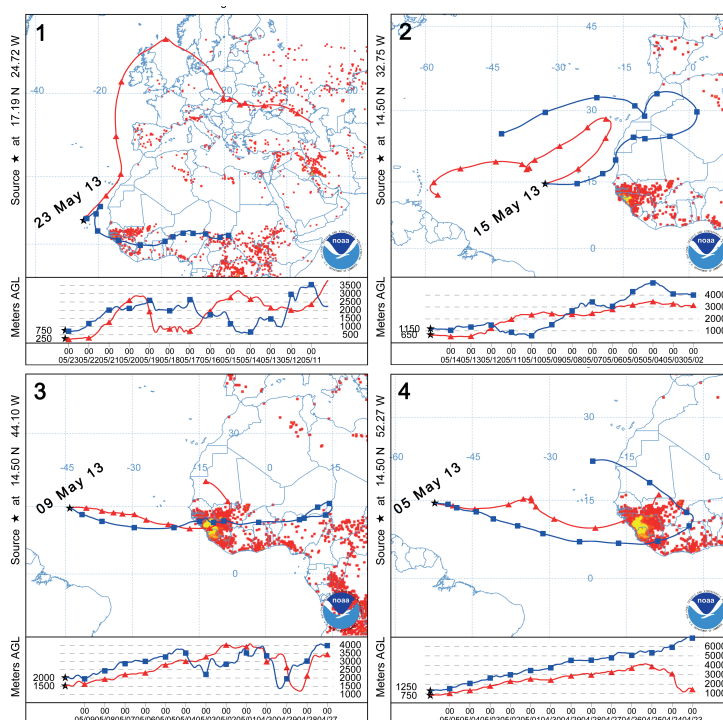
23

Figure 10. 13-day backward trajectories for the same cases as in Fig. 5 and arrival heights 250 m below (red) and 250 m above the SAL base height.